Control of the orbital character of indirect excitons in MoS_{2}/WS_{2} heterobilayers

Jonas Kiemle, Florian Sigger, Michael Lorke, Bastian Miller, Kenji Watanabe, Takashi Taniguchi, Alexander Holleitner, and Ursula Wurstbauer

Phys. Rev. B **101**, 121404 — Published 18 March 2020

DOI: 10.1103/PhysRevB.101.121404

Control of the orbital character of indirect excitons in MoS_2/WS_2 heterobilayers

Jonas Kiemle,[1] Florian Sigger,[1] Michael Lorke,[2,3] Bastian Miller,[1] Kenji Watanabe,[4] Takashi Taniguchi,[4] Alexander Holleitner,[1,5] and Ursula Wurstbauer[1,5,6,*]

[1] *Walter Schottky Institut and Physics Department, Technical University of Munich, Am Coulombwall 4a, 85748 Garching, Germany*
[2] *Bremen Center for Computational Materials Science, University of Bremen, Am Fallturm 1, 28359 Bremen, Germany*
[3] *Institute for Theoretical Physics, University of Bremen, 28359 Bremen, Germany*
[4] *National Institute for Materials Science, Tsukuba, Ibaraki 305-0044, Japan*
[5] *Nanosystems Initiative Munich (NIM), Schellingstr. 4, 80799 München, Germany*
[6] *Institute of Physics, Westfälische Wilhelms-Universität Münster, Wilhelm-Klemm-Str.10, 48149 Münster, Germany*

(Dated: 2020-03-03)

Valley selective hybridization and residual coupling of electronic states in commensurate van der Waals heterobilayers enable the control of the orbital character of interlayer excitons. We demonstrate electric field control of layer index, orbital character, lifetime and emission energy of indirect excitons in MoS_2/WS_2 heterobilayers embedded in an vdW field effect structure. Different excitonic dipoles normal to the layers are found to stem from bound electrons and holes located in different valleys of MoS_2/WS_2 with a valley selective degree of hybridization. For the energetically lowest emission lines, coupling of electronic states causes a field-dependent level anticrossing that goes along with a change of the IX lifetime from 400 ns to 100 ns. In the hybridized regime the exiton is delocalized between the two constituent layers, whereas for large positive or negative electric fields, the layer index of the bound hole is field-dependent. Our results demonstrate the design of novel van der Waals solids with the possibility to in-situ control their physical properties via external stimuli such as electric fields.

Van der Waals (vdW) heterobilayers (HBs) prepared from optically active transition metal dichalcogenide (TMDC) monolayers, such as MoS_2 or WS_2, combine the excellent properties of the individual layers with the potential for novel functionality provided by the full control of vdW architecture [1–7]. By stacking two different TMDC monolayers, the electronic bands form an atomically sharp p-n heterojunction, effectively separating photo-generated electron-hole pairs [2, 8, 9]. This charge transfer allows for the formation of so-called interlayer excitons (IXs) with electrons and holes residing in different layers [10, 11]. The reduced overlap of the electron-hole wavefunctions entails greatly prolonged exciton lifetimes of more than 100 ns [10, 12], exceeding the lifetime of intralayer excitons by several orders of magnitude [13, 14], as previously reported for IX in in tunnel coupled GaAs QW structures [15]. The long lifetimes enable the formation of thermalized dense exciton ensembles [16], which, together with IX diffusion over several micrometers [17, 18], sets up the possibility to operate excitonic devices [17, 19].

Due to hybridization, moiré effects and altered dielectric environment [2–6, 20, 21], real TMDC HBs can have a much more complicated band structure with fascinating and so far only little explored electronic and optical properties based on the orbital character of the involved electronic states. For the HBs embedded in a field-effect device, an anti-crossing behaviour of IXs is expected based on the residual coupling of electronic states in the two TMDC layers [20] accompanied by a gradual change of the exciton nature from primarily interlayer to primarily intralyer [cf. Figure 1a]. Since such a coherent coupling occurs across the vdW gap, the field-tunable degree of hybridization and therefore, layer index of electronic states in MoS_2/WS_2 HBs opens the door for straight-forward design and fabrication of novel quantum materials, e.g. for the realization of charge qubits in stacked field-effect devices [22]. Here, we demonstrate the electrical field control of the IXs in MoS_2/WS_2 HBs and we find a field-dependent level anti-crossing of the energetically lowest IX emission lines in low-temperature (10K) photoluminescence (PL) [cf. Figure 1b,c]. Field dependent level anti-crossing has also been reported for coupled quantum dots originating from Coulomb mediated hybridization of excitons [23] and not of orbital states as in the present work on vdW hetero-bilayers. The temperature dependence of the PL in combination with dipole moments from the Stark shift measurements allow the classification of the involved orbital states in MoS_2/WS_2 HBs. The observed hybridization effects suggest that vdW HB need to be treated as artificial vdW solids.

The relative band alignment of the two layers of the MoS_2/WS_2 HBs responds linearly vs an electric field $\boldsymbol{F}$ as $E_{MoS_2}(F) - E_{WS_2}(F) = E_{MoS_2}(0) - E_{WS_2}(0) - eFd/\varepsilon$, where E_{MoS_2} and E_{WS_2} are the band energies of the single layers, Fd describes the voltage drop across the HB and ε is the effective dielectric function[20]. Without finite interlayer coupling, the VB states of the two bands at K would pass through each other. The projection of the electronic wave function on either layer at

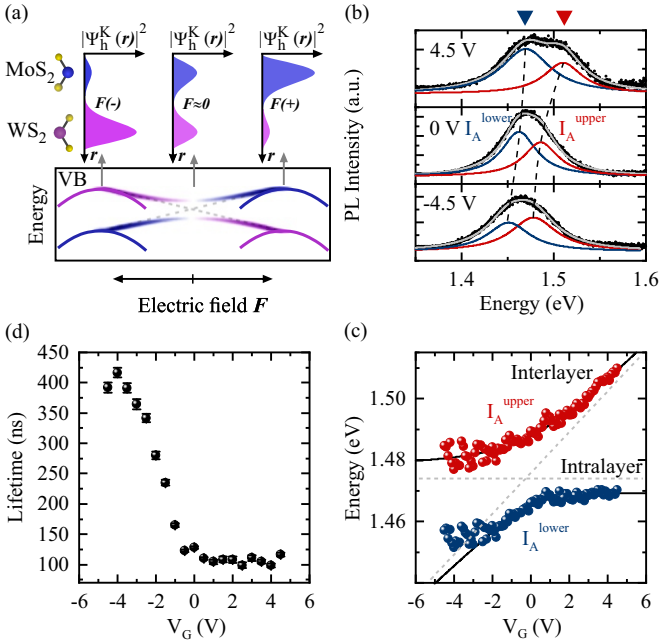

FIG. 1. (a) Schematic depiction of the squared moduli of the hole wave-functions of the MoS_2/WS_2 HB at the topmost VB state at the K point $|\psi_h^K(\boldsymbol{r})|^2$ for large negative $\boldsymbol{F}(-)$, vanishing $\boldsymbol{F} \approx 0$ and large positive electric fields $\boldsymbol{F}(+)$. The coupling of electronic hole states result in a field-tunable hybridization and anti-crossing behavior of the valence band states at the K^{VB}-point. (b) PL spectra at 10 K for applied voltages V_G of −4.5 V, 0 V and 4.5 V. (c) Emission energy of upper and lower exciton branch as a function of V_G indicating the anti-crossing behaviour. The gray dashed lines indicate the interlayer and intralayer character of the exciton emission. (d) PL lifetime of the $I_{\mathrm{A}}^{\mathrm{lower}}$ emission line as a function of V_G, measured at a bath temperature of 10 K. [sample 1]

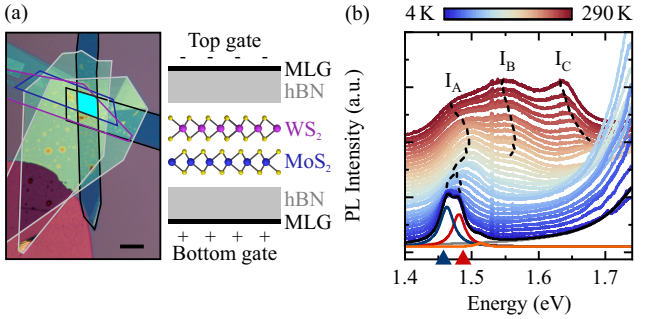

FIG. 2. (a) Optical microscope image and schematic depiction of the device structure. The turquoise area indicates the HB area. Scale bar is 10 µm [sample 1]. (b) IX PL spectra for bath temperatures between 290 K (dark red) and 4 K (dark blue). The black dashed lines are guides to the eye indicating the emission energy of IXs I_{A}, I_{B} and I_{C}. [sample 2].

the reciprocal point $K_{\mathrm{WS_2}}^{\mathrm{VB1}}$ contains about 10 % of MoS_2, and $K_{\mathrm{MoS_2}}^{\mathrm{VB2}}$ contains 10 % of WS_2[20, 21, 24]. The finite coupling causes level repulsion which manifests in an avoided crossing [20] of the IX emission energies [Figure 1a]. These VB states bind to electronic states at the conduction band (CB) $\Sigma_{\mathrm{HB}}^{\mathrm{CB}}$ that are delocalized between the MoS_2 (75 %) and WS_2 (25 %)[20, 21, 24] monolayers forming IXs. The solid line plotted in Figure 1d quantifies the coupling strength γ of these IXs using a simplified model of a coupled two-level system

$$E_{\pm} = \frac{1}{2}(\Delta(0) - eFd/\varepsilon) \pm \sqrt{(\Delta(0) - eFd/\varepsilon)^2 + 4\gamma^2},$$

where $E_{\pm}$ denotes the upper (+) and lower (-) energy branch and $\Delta(0) = E_{\mathrm{MoS_2}}(0) - E_{\mathrm{WS_2}}(0)$ [20]. The model fit to the data yields $\gamma_+ = 11$ meV and $\gamma_- = 5$ meV for the upper and lower branch, respectively. We assume this asymmetry to result from the unequal hybridization at $\Sigma_{\mathrm{HB}}^{\mathrm{CB}}$ with 75 % MoS_2 and 25 % WS_2[20, 21, 24]. As a direct consequence of the avoided crossing, the excitons $I_{\mathrm{A}}^{\mathrm{lower}}$ gradually change their nature from interlayer, to an intralayer exciton of the artificial van der Waals solid in the anti-crossing regime with delocalized electron at $\Sigma_{\mathrm{HB}}^{\mathrm{CB}}$ and delocalized hole at $K_{\mathrm{HB}}^{\mathrm{VB}}$. Further increasing the positive gate voltage gradually turns the nature of the exciton back to an IX. This appears analogously for $I_{\mathrm{A}}^{\mathrm{upper}}$. In this interpretation, the hole changes its hosting layer, too. For the lowest energy emission line, the hole is localized in WS_2 for large negative gate voltages and localized in MoS_2 for large positive gate voltages. Due to the altered overlap of the electron and the hole wave-function, we expect also the lifetime of the excitons to depend strongly on the applied voltage V_G. Indeed, voltage-dependent lifetime measurements of the lowest emission line reveal that the lifetime is about 400 ns for negative voltages, where the wave-function overlap should be smallest. The lifetime decreases to about 100 ns for zero voltage and saturates for larger voltages as shown in Figure 1d. We explain the saturation in lifetime by the similar overlap of electron and hole wave-functions in the hybridized regime (small voltages) and for the hole localized in MoS_2 (positive voltages).

The devices in this study consist of almost lattice matched [25] MoS_2 and WS_2 monolayers encapsulated with few-layer hBN and sandwiched between graphite bottom- and top-gate electrodes. The HBs are prepared by micromechanical exfoliation and an all-dry viscoelastic stamping method [26]. A monolayer WS_2 is stacked onto a monolayer MoS_2 such that the crystal axes are rotationally aligned to 0° or 60° with a precision of about ±0.5° [24]. A total of 8 hBN-encapsulated MoS_2/WS_2 HBs have been fabricated and characterized [24]. The behaviour of the different devices is consistent and the devices are exceptionally robust against thermal cycling, storage in nitrogen and repeated measurements over months. Even for lowest excitation intensities and low temperatures, we do not observe signatures of moiré excitons [3, 4, 6]. An optical micrograph and a schematic of the device are shown in Figure 2a. Figure 2b depicts a temperature series of typical PL spectra

taken in a temperature range between room temperature (topmost trace) and 4K (lowest trace). The measurements were carried out using an excitation energy of $E_{laser} = 2.54\,eV$ and a power of $P_{laser} = 100\,\mu W$, corresponding to about $10\,kW/cm^2$ (spot-size $1\,\mu m$). The emission intensities towards higher energies belong to the direct excitons of WS_2 and MoS_2[see SI]. The well resolved triplet-structure at higher temperatures occurring between 1.4 eV and 1.7 eV is interpreted to stem from IXs in agreement with a recent report by Okada *et al.* [27]. For a non-hBN encapsulated MoS_2/WS_2 HB, the triplet structure cannot be well resolved [24] revealing the importance of hBN encapsulation for narrow emission bands [28, 29]. Direct comparison of different samples indicate that the formation of IXs in TMDC HBs does not dependent on the 0° or 60° alignment in agreement with recent reports in literature [4, 27, 30], see Supplemental Material for additional data [24] together with Refs. [31–35]. To quantitatively analyze the evolution of the IX emission with temperature the spectra are described by an adequate sum of peak-profiles as exemplary shown for the spectrum at the lowest temperature. The evolution of the IX emission energies with temperature is summarized in Figure 3a. As expected from an increasing single particle band gap with decreasing temperature, the emission energy of I_C increases monotonously, similar to the direct excitons (not shown). The emission energy of I_B is almost constant and the intensity continuously decreases with decreasing temperature, becoming indistinguishable from the noise level below 100 K. The emission energy of I_A has a very broad maximum around 150 K. The 4 K spectrum in Figure 2b clearly demonstrates, that the line splits into a well resolved doublet structure labeled with I_A^{lower} and I_A^{upper} at temperatures below 40 K. Notably, below 30 K another weak emission line I_D appears energetically just above I_A^{upper}.

Figure 3b depicts the evolution of the peak position of the IX multiplet from Lorentzian fits to the spectra in the presence of an external electric field at room temperature. Therefore a voltage V_G is applied between top and bottom graphene electrodes (left axis). Within the considered range of applied voltages, the IX contributions exhibit linear Stark shifts ΔE of different magnitudes almost independent from the temperature [not shown]. We attribute the non-uniform shifts of the three IX signatures to different out-of-plane dipole moments μ_0. In dependence on the electric field $\boldsymbol{F}$, the Stark shift is given by $\Delta E = \mu_0 \boldsymbol{F} + \alpha \boldsymbol{F}^2$, where $\mu_0 = e d_0$ is the intrinsic dipole moment, d_0 denotes the distance between electron and hole and α is the polarizability of the exciton. Because of the vertical separation of electron and hole, we assume the linear term to be the dominating contribution to the Stark shift. This assumption is in agreement with the experimentally observed linear slopes of the PL peak energies with varying voltage V_G [see Figure 3b]. The unequal values of μ_0 indicate different separations of the

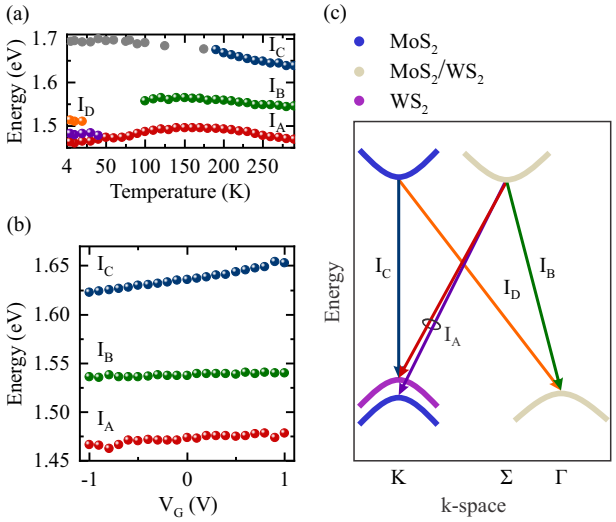

FIG. 3. (a) Emission energies of IXs I_A, I_B, I_C, and I_D as a function of bath temperature. [sample 2, grey solid dots of the I_C branch sample 1]. (b) Voltage-dependent emission energies of IXs at room temperature. [sample 1]. (c) Schematic band structure of a MoS_2/WS_2 HB projected onto the atomic orbitals of the individual layers. Blue and purple band colors correspond to MoS_2 and WS_2 monolayers, while light beige color denotes a large degree of hybridization. The anticipated optical interband transitions are marked by arrows.

electron-hole pairs along the direction of $\boldsymbol{F}$. This is consistent with distinctively different orbital compositions of the electronic states in k-space contributing to the excitonic transitions of the MoS_2/WS_2 HB. The Stark shifts at room temperature for the three IX transitions are 15.1 meV/V for I_C, 2.5 meV/V for I_B, and 6.3 meV/V for I_A. The estimated separation of the electron and hole along the electric field constitute approximately 1.8 Å, 0.3 Å and 0.8 Å for I_C, I_B and I_A, respectively. The low temperature values for the stark shifts ΔE at 4 K are very similar to the values at room temperatures and are 17.0 meV/V for I_C and ≈ 7 meV/V for I_A^{lower}, I_A^{upper} and I_D, respectively.

The peculiar temperature dependence together with the significantly different Stark shifts strongly suggest that the IXs are formed by electrons and holes residing in different valleys of the BZ. The conduction (CB) and valence bands (VB) of the MoS_2/WS_2 HB near the relevant critical points at the Γ, K and Σ valleys are sketched in Figure 3c following recent theoretical work [20, 21, 24]. The single particle bands are projected onto the atomic orbitals of the individual layers that are reflected by the color code. Red and blue colors correspond to electronic states purely from MoS_2 and WS_2, respectively, whereas light beige indicates hybridization of states from both layers. The hybridization is a consequence of coupling between electronic states on the molecular-orbital level that is particularly strong at the Σ valley in the CB and the Γ valley in the VB. From DFT calculations, the rele-

vant high symmetry points of the band structure appear to be similar for AB and AA stacked MoS_2/WS_2 HBs [24].

The lowest CB states at the K^{CB}-point are of 100 % MoS_2 character, whereas the two topmost VB states at the K^{VB}-point are split by only ≈ 16 meV and are of inverse orbital character with around 90 % WS_2 and 90 % MoS_2 for the higher and lower state [24]. Similar to TMDC homo-bilayers, also the MoS_2/WS_2 HBs are indirect semiconductors with the lowest energy transition between the Σ^{CB} and the K^{VB} valley [21].

Due to of the strong hybridization of the electronic states for some high symmetry points, those electrons and holes are delocalized between the two layers and, hence, behave more like charge carriers of a new 'artificial vdW solid' than of a vdW HB. Guided by this aspect, we assign the emission line of I_B with smallest Stark shift and consequently the smallest separation between electron-hole pairs, to be formed by an electron at Σ^{CB}_{HB} and a hole at Γ^{VB}_{HB}. The small but finite vertical separation of the charge carriers results from a large degree of orbital hybridization with approx. 75 % MoS_2 character at the Σ^{CB}-point and approx. 60 % WS_2 character at the Γ^{VB} point[20, 24]. Therefore, I_B can be interpreted as momentum indirect, but real space more direct transition of the MoS_2/WS_2 vdW solid. With similar arguments, we assign I_C, which shows the largest Stark shift to be an IX with the electron in the fully layer polarized $K^{CB}_{MoS_2}$-point (≈ 100 % MoS_2[20]) and the hole in the almost fully layer polarized $K^{VB1}_{WS_2}$-point (≈ 90 % WS_2[20]). The remaining excitons I_A and I_D exhibit all similar Stark shift values that are between those of I_C and I_B. For this reason, it is most likely that for these interband transitions one of the charge carriers is more delocalized between the two layers and resides in a highly hybridized valley, while the other coulomb coupled charge carrier is localized in either MoS_2 or WS_2 and belongs therefore to a non- or only weakly hybridized valley.

Taking into account the energies of the IXs with $E(I_D) > E(I^{upper}_A) > E(I^{lower}_A)$, we assign I_D to the transition with the electron at $K^{CB}_{MoS_2}$ and the hole at the hybridized Γ^{VB}_{HB}-point. The lowest energy emission lines I^{lower}_A and I^{upper}_A are those showing anti-crossing behaviour in electric field-dependent measurements. The experimentally found energy separation of the two emission lines is about 20 meV which is in excellent agreement with the theoretical value of about 16 meV obtained from DFT calculation [24]. In brief, the five red-shifted emission lines are assigned to a momentum direct interlayer transition I_C from $K^{CB}_{MoS_2}$ to $K^{VB1}_{WS_2}$, a momentum indirect intralayer transition I_B from Σ^{CV}_{HB} to Γ^{VB}_{HB} and three momentum indirect interlayer transitions, namely I^{lower}_A from Σ^{CB}_{HB} to $K^{VB1}_{WS_2}$, I^{upper}_A from Σ^{CB}_{HB} to $K^{VB2}_{MoS_2}$ and I_D from $K^{CB}_{MoS_2}$ to Γ^{VB}_{HB}.

The increase of the emission energy of I_C with decreasing temperature between 290 K and 150 K is consistent with an increase of the single particle band gap of both constituent layers [36]. The subsequent lowering of the emission energy below 150 K and reduced emission intensity might be caused by a reduction of the amount of thermally excited kinematic excitons with $|\Delta k| > 0$ that can couple to the light, since we expect a slight lattice mismatch to cause a slight misalignment of the MoS_2 and WS_2 K-points [12, 24, 37]. The slight mismatch in the momenta at this quasi direct interband transition at the K-points might also be the reason for the reduced emission intensity with reduced temperature. The phonon-activated transition I_B is rather broad and disappears below about 100 K, which is expected to be caused by the combined effect of reduced electron-phonon coupling and freezing of the relevant phonon modes [38].

To conclude, we demonstrate widely tunable IX emission by applying an electric field perpendicular to the HB plane. The results are interpreted in terms of finite interlayer coupling, resulting in different orbital hybridization dominating the multiphysics of IX transitions in MoS_2/WS_2 HBs. Most remarkably, the field-tunable anti-crossing behaviour of the lowest IX emission lines goes along with a field-dependent change of the exciton character from interlayer to intralayer and back to interlayer, accompanied with a transfer of the participating hole between the constituent layers. These types of HBs enable the realization of a new type of charge qubits [22]. The observed valley-dependent hybridization effects manifest that vdW HBs need to be treated as artificial vdW solids.

We gratefully acknowledge financial support by the Deutsche Forschungsgemeinschaft (DFG) via excellence cluster 'Nanosystems Initiative Munich' (NIM) and DFG projects WU 637/4- 1 and HO 3324/9-1. M.L. was supported by the Deutsche Forschungsgemeinschaft (DFG) within RTG 2247 and through a grant for CPU time at the HLRN (Hannover/Berlin). K.W. and T.T. acknowledge support from the Elemental Strategy Initiative conducted by the MEXT, Japan and and the CREST (JPMJCR15F3), JST.

* wurstbauer@wwu.de

[1] A. K. Geim and I. V. Grigorieva, Nature **499**, 419 (2013).
[2] P. Rivera, H. Yu, K. L. Seyler, N. P. Wilson, W. Yao, and X. Xu, Nature nanotechnology **13**, 1004 (2018).
[3] C. Jin, E. C. Regan, A. Yan, U. M. Iqbal Bakti, D. Wang, S. Zhao, Y. Qin, S. Yang, Z. Zheng, S. Shi, K. Watanabe, T. Taniguchi, S. Tongay, A. Zettl, and F. Wang, Nature **567**, 76 (2019).
[4] E. M. Alexeev, D. A. Ruiz-Tijerina, M. Danovich, M. J. Hamer, D. J. Terry, P. K. Nayak, S. Ahn, S. Pak, J. Lee, J. I. Sohn, M. R. Molas, M. Koperski, K. Watanabe, T. Taniguchi, K. S. Novoselov, R. V. Gorbachev, H. S. Shin, V. I. Fal'ko, and A. I. Tartakovskii, Nature **567**,

81 (2019).
[5] K. L. Seyler, P. Rivera, H. Yu, N. P. Wilson, E. L. Ray, D. G. Mandrus, J. Yan, W. Yao, and X. Xu, Nature **567**, 66 (2019).
[6] K. Tran, G. Moody, F. Wu, X. Lu, J. Choi, K. Kim, A. Rai, D. A. Sanchez, J. Quan, A. Singh, J. Embley, A. Zepeda, M. Campbell, T. Autry, T. Taniguchi, K. Watanabe, N. Lu, S. K. Banerjee, K. L. Silverman, S. Kim, E. Tutuc, L. Yang, A. H. Macdonald, and X. Li, Nature **567**, 71 (2019).
[7] Z. Wang, D. A. Rhodes, K. Watanabe, T. Taniguchi, J. C. Hone, J. Shan, and K. F. Mak, Nature **574**, 76 (2019).
[8] X. Zhu, N. R. Monahan, Z. Gong, H. Zhu, K. W. Williams, and C. A. Nelson, Journal of the American Chemical Society **137**, 8313 (2015).
[9] H. Chen, X. Wen, J. Zhang, T. Wu, Y. Gong, X. Zhang, J. Yuan, C. Yi, J. Lou, P. M. Ajayan, W. Zhuang, G. Zhang, and J. Zheng, Nature communications **7**, 12512 (2016).
[10] P. Rivera, J. R. Schaibley, A. M. Jones, J. S. Ross, S. Wu, G. Aivazian, P. Klement, K. Seyler, G. Clark, N. J. Ghimire, J. Yan, D. G. Mandrus, W. Yao, and X. Xu, Nature communications **6**, 6242 (2015).
[11] P. Rivera, K. L. Seyler, H. Yu, J. R. Schaibley, J. Yan, D. G. Mandrus, W. Yao, and X. Xu, Science **351**, 688 (2016).
[12] B. Miller, A. Steinhoff, B. Pano, J. Klein, F. Jahnke, A. Holleitner, and U. Wurstbauer, Nano letters **17**, 5229 (2017).
[13] C. Robert, D. Lagarde, F. Cadiz, G. Wang, B. Lassagne, T. Amand, A. Balocchi, P. Renucci, S. Tongay, B. Urbaszek, and X. Marie, Physical Review B **93**, 205423 (2016).
[14] M. Palummo, M. Bernardi, and J. C. Grossman, Nano letters **15**, 2794 (2015).
[15] A. Gärtner, A. W. Holleitner, J. P. Kotthaus, and D. Schuh, Applied Physics Letters **89**, 052108 (2006).
[16] P. Nagler, G. Plechinger, M. V. Ballottin, A. Mitioglu, S. Meier, N. Paradiso, C. Strunk, A. Chernikov, P. C. M. Christianen, C. Schüller, and T. Korn, 2D Materials **4**, 025112 (2017).
[17] D. Unuchek, A. Ciarrocchi, A. Avsar, K. Watanabe, T. Taniguchi, and A. Kis, Nature **560**, 340 (2018).
[18] M. Kulig, J. Zipfel, P. Nagler, S. Blanter, C. Schüller, T. Korn, N. Paradiso, M. M. Glazov, and A. Chernikov, Physical review letters **120**, 207401 (2018).
[19] L. A. Jauregui, A. Y. Joe, K. Pistunova, D. S. Wild, A. A. High, Y. Zhou, G. Scuri, K. de Greve, A. Sushko, C.-H. Yu, T. Taniguchi, K. Watanabe, D. J. Needleman, M. D. Lukin, H. Park, and P. Kim, arXiv (2018).
[20] S. Gao, L. Yang, and C. D. Spataru, Nano letters **17**, 7809 (2017).
[21] T. Deilmann and K. S. Thygesen, Nano letters **18**, 1460 (2018).
[22] B. Lucatto, D. S. Koda, F. Bechstedt, M. Marques, and L. K. Teles, "Charge qubit in van der waals heterostructures," .
[23] P.-L. Ardelt, K. Gawarecki, K. Müller, A. M. Waeber, A. Bechtold, K. Oberhofer, J. M. Daniels, F. Klotz, M. Bichler, T. Kuhn, H. J. Krenner, P. Machnikowski, and J. J. Finley, Physical review letters **116**, 077401 (2016).
[24] See Supplemental Material at [URL] for a description of the sample preparation, additional data on time-integrated gate-tunable PL and time-resolved gate-tunable PL, density functional calculation, and a table with orbital compositions of Bloch states at certain high symmetry points..
[25] J. A. Wilson and A. D. Yoffe, Advances in Physics **18**, 193 (1969).
[26] A. Castellanos-Gomez, M. Buscema, R. Molenaar, V. Singh, L. Janssen, H. S. J. van der Zant, and G. A. Steele, 2D Materials **1**, 011002 (2014).
[27] M. Okada, A. Kutana, Y. Kureishi, Y. Kobayashi, Y. Saito, T. Saito, K. Watanabe, T. Taniguchi, S. Gupta, Y. Miyata, B. I. Yakobson, H. Shinohara, and R. Kitaura, ACS nano **12**, 2498 (2018).
[28] J. Wierzbowski, J. Klein, F. Sigger, C. Straubinger, M. Kremser, T. Taniguchi, K. Watanabe, U. Wurstbauer, A. W. Holleitner, M. Kaniber, K. Müller, and J. J. Finley, Scientific reports **7**, 12383 (2017).
[29] F. Cadiz, E. Courtade, C. Robert, G. Wang, Y. Shen, H. Cai, T. Taniguchi, K. Watanabe, H. Carrere, D. Lagarde, M. Manca, T. Amand, P. Renucci, S. Tongay, X. Marie, and B. Urbaszek, Physical Review X **7**, 021026 (2017).
[30] P. K. Nayak, Y. Horbatenko, S. Ahn, G. Kim, J.-U. Lee, K. Y. Ma, A.-R. Jang, H. Lim, D. Kim, S. Ryu, H. Cheong, N. Park, and H. S. Shin, ACS nano **11**, 4041 (2017).
[31] J. Kunstmann, F. Mooshammer, P. Nagler, A. Chaves, F. Stein, N. Paradiso, G. Plechinger, C. Strunk, C. Schüller, G. Seifert, D. R. Reichman, and T. Korn, Nature Physics **14**, 801 (2018).
[32] L. M. Malard, T. V. Alencar, A. P. M. Barboza, K. F. Mak, and A. M. de Paula, Physical Review B **87**, 201401 (2013).
[33] N. Kumar, S. Najmaei, Q. Cui, F. Ceballos, P. M. Ajayan, J. Lou, and H. Zhao, Physical Review B **87**, 161403 (2013).
[34] L. Mennel, M. Paur, and T. Mueller, APL Photonics **4**, 034404 (2019).
[35] G. Kresse and D. Joubert, Phys. Rev. B **59**, 1758 (1999).
[36] Y. P. Varshni, Physica **34**, 149 (1967).
[37] H. Yu, Y. Wang, Q. Tong, X. Xu, and W. Yao, Physical review letters **115**, 187002 (2015).
[38] Y. Ge and A. Y. Liu, Physical Review B **87**, 241408(R) (2013).